Check for updates

Received: 27 February 2023 | Revised: 17 May 2023 | Accepted: 23 May 2023

DOI: 10.1002/jcc.27173

RESEARCH ARTICLE

Journal of COMPUTATIONAL CHEMISTRY WILEY

Performance of the COSMO solvation model for photoacidity and basicity in water

Ali Ghiami-Shomami | Christof Hättig

Lehrstuhl für Theoretische Chemie, Ruhr-Universität Bochum, Bochum, Germany

Correspondence
Christof Hättig, Lehrstuhl für Theoretische Chemie, Ruhr-Universität Bochum, D-44780 Bochum, Germany.
Email: christof.haettig@rub.de

Funding information
Deutsche Forschungsgemeinschaft

Abstract

The possibilities and problems to predict excited-state acidities and basicities in water with electronic structure calculations combined with a continuum solvation model are investigated for a test set of photoacids and photobases. Different error sources, like errors in the ground-state pK_a values, the excitation energies in solution for the neutral and (de-)protonated species, basis set effects, and contributions beyond implicit solvation are investigated and their contributions to the total error in pK_a^* are discussed. Density functional theory in combination with the conductor like screening model for real solvents and an empirical linear Gibbs free energy relationship are used to predict the ground-state pK_a values. For the test set, this approach gives more accurate pK_a values for the acids than for the bases. Time-dependent density-functional theory (TD-DFT) and second-order wave function methods in combination with the conductor like screening model are applied to compute excitation energies in water. Some TD-DFT functionals fail for several species to predict correctly the order of the lowest excitations. Where experimental data for absorption maxima in water is available, the implicit solvation model leads with the applied electronic structure methods in most cases for the excitation energies in water to an overestimation for the protonated and to an underestimation for the deprotonated species. The magnitude and sign of the errors depend on the hydrogen bond donating and accepting ability of the solute. We find that for aqueous solution this results generally in an underestimation in the pK_a changes from the ground to the excited state for photoacids and an overestimation for photobases.

KEYWORDS
ADC(2), CC2, COSMO, excitation energies, photoacids, photobases, solvent effects, TD-DFT

1 | INTRODUCTION

Proton transfer is one of the most fundamental processes in nature that plays vital roles in chemical and biological processes both in the ground state (GS) and in excited states (ES). However, the acidic or basic properties of compounds in excited states are often considerably different from those in the ground state, as a result of the changes in the electron distribution induced by the transition. Excited-state proton transfer reactions in solution can be either of the excited-state intermolecular proton transfer (ESPT) or the excited-state intra-molecular proton transfer (ESIPT) type.[1] In ESPT, which is the subject of the current paper, a proton is transferred from one molecule to another molecule, for example, form a solute to the solvent or vice versa. Compounds that become strong acids or bases only upon irradiation are called, respectively, photoacids or photobases. This process can be irreversible when the irradiation initiates an

This is an open access article under the terms of the Creative Commons Attribution-NonCommercial License, which permits use, distribution and reproduction in any medium, provided the original work is properly cited and is not used for commercial purposes.
© 2023 The Authors. *Journal of Computational Chemistry* published by Wiley Periodicals LLC.

irreversible photochemical reaction that produces the acid or base, or it can be reversible which is the case when the acid strength in the excited state (pK_a^*) is considerably decreased or increased relative to the ground state value (pK_a) of a weak acid or base. Reversible photoacids or bases are often desirable since the proton transfer process can be initiated by turning light on and off, thus achieving a high degree of control over the process. Knowledge of pK_a^* and an understanding of the factors that influence it in solution is vital in designing new photoacid and bases.[2,3] The most accurate experimental method of determining pK_a^* of a photoacid or base is the direct kinetic measurement of the excited-state proton dissociation and recombination rates.[4-6] However, these measurements are not trivial and are limited to a relatively small number of photoacids where accurate measurement of the excited-state reversible dynamics of the proton-transfer reaction is possible.[7] An indirect determination via the thermodynamic Förster cycle[8,9] appears to be the most general applicable way for estimating pK_a^* values using the ground state acid strengths (pK_a) and the electronic transition energies of the protonated and deprotonated species in solution.[8] From an experimental point of view, UV/vis absorption and fluorescence spectroscopy is usually used to determine the transition energies of photoacids and bases that are needed to estimate the pK_a^* values.[2,3] However, pK_a^* measurements are not always practical—especially when the ESPT process is fast or the excited-state lifetime is short. Therefore, computational methods for determining pK_a^* are desirable. They would also be useful for predicting excited-state acid strengths of newly proposed photoacids or bases and help to decide if it is worth the effort to synthesize them.

While there are established and validated procedures like thermodynamic cycles for computing ground-state pK_a values, the prediction of pK_a^* by computational chemistry is still hampered by the lack of accurate methods for electronic transition energies in solution. This arises from limitations for the modeling of excited-state solvation with accurate electronic structure methods. In fact, only few papers on the prediction of excited-state acidities and basicities of photoacids and photobases using quantum mechanical methods are available in the literature (see e.g., References 10-18 and references cited therein). For predicting pK_a^* via the Förster cycle, the ground-state pK_a value and the transition energies of the acid and the base need to be calculated in solution. Alternatively, also the Born-Haber cycle can be used, which splits the contributions to pK_a^* in a different way[16] so that separate methods can be used to compute gas-phase excitation energies and excited-state solvation free energies ΔG_{solv}. This approach allows a more strict comparison with experimental results from direct kinetic measurements and has very successfully been applied in calculations on coumarins.[16] However, results for pK_a^* from direct kinetic measurements are limited to a relatively small number of photoacids.[7] Therefore, we used for the calculations reported in the current work the Förster cycle which can directly be compared with experimental results using this thermodynamic cycle which are more abundant.

Popular electronic structure methods used for computing excitation energies as one of the quantities necessary for computing excited state acidities and basicities are time-dependent density functional theory[19] (TD-DFT) and also wavefunction methods like coupled cluster response methods and multireference perturbation and configuration interaction.[20] While TD-DFT methods within the adiabatic approximation are computationally cheaper than most wavefunction methods, they often have problems to describe accurately charge-transfer transitions,[20] depending on the functional. Several popular functionals also fail more often than correlated wavefunction methods to reproduce the correct order of the lowest $n\pi^*$ and $\pi\pi^*$ transitions in aromatic organic compounds.[21,22] However, almost all of the available computational studies on photoacidity are limited to TD-DFT although intra-molecular charge-transfer and its interplay with the aromaticity plays an important role for the photoacidity of aromatic compounds.[23] An exception is a recent investigation of the photoacidity of hydroxypyrenes in dimethyl sulfoxide by Sülzner and Hättig[18] that employed second-order wavefunction methods in combination with a continuum solvation model.

Since pK_a^* depends directly on the difference between the excitation energies of the acid and its conjugated base, the accuracy of computational results depends crucially on a balanced description of the latter in solution, which is in particular for protic solvents challenging.

In this work, excitation energies and pK_a^* values for a test set of photoacids and photobases are computed for water as the most important solvent and compared to experimental excitation energies and pK_a^* values. The aim is to investigate systematically the influence of computational parameters like the electronic structure method (TD-DFT with different functionals and second-order wavefunction methods), geometries, and basis sets on pK_a^* and the limitations of continuum solvation models. For the latter we use the conductor-like screening model[24] (COSMO) as example. This choice is motivated by the availability of COSMO for the algebraic diagrammatic construction scheme through second order,[25-27] ADC(2), and the approximate coupled-cluster singles-and-doubles method[28,29] CC2 and its relation to the conductor-like screening model for real solvents[30] (COSMO-RS) that is used for ground-state pK_a values.

2 | TEST SET AND METHODOLOGY

The test set we chose for the current study comprises of a set of twelve photoacids which includes phenols, naphthols, and hydroxycoumarins (see Figure 1) and a set of eight photobases consisting of quinolines and acridine (see Figure 2). They have been selected to include in the test set the most important known categories of photoacids and bases with available experimental acidity or basicity values in the ground and excited states.

For the calculation of the ground-state pK_a values, first, a conformational analysis has been performed for all compounds that could have more than one conformer using the COSMO*conf* software.[31] For all conformers the geometries have first been optimized at the BP86/def-TZVP level[32-34] of theory in combination with the conductor like screening model (COSMO) and a value of 78.3 for the dielectric constant of water.[35] All DFT calculations have been carried out using the

1096987x, 2023, 24, Downloaded from https://onlinelibrary.wiley.com/doi/10.1002/jcc.27173 by Ruhr-Universität Bochum, Wiley Online Library on [09/10/2023]. See the Terms and Conditions (https://onlinelibrary.wiley.com/terms-and-conditions) on Wiley Online Library for rules of use; OA articles are governed by the applicable Creative Commons License

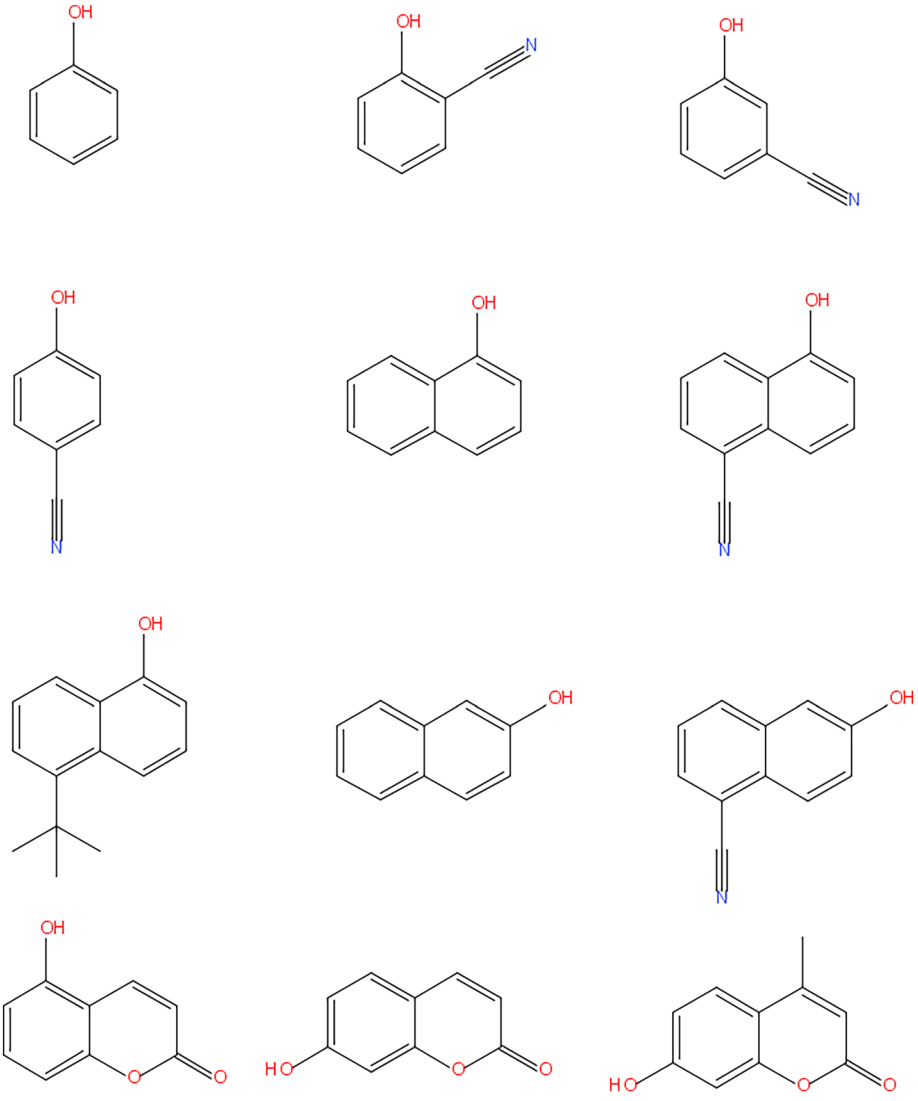


FIGURE 1 Structures of the photoacids studied in this work.

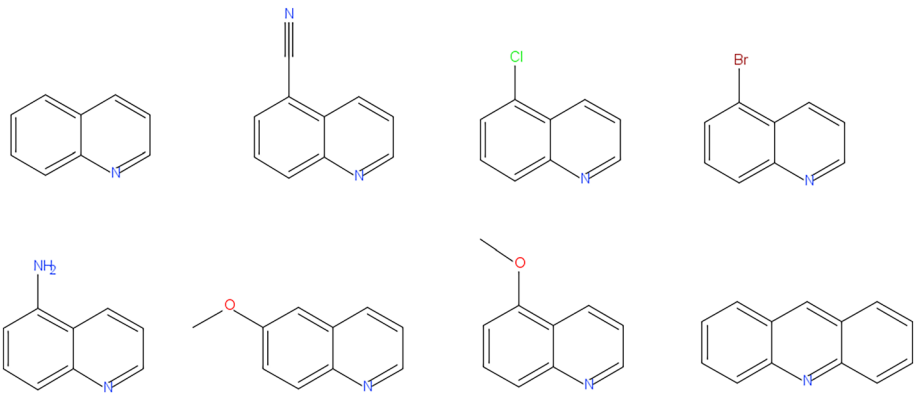


FIGURE 2 Structures of the photobases studied in this work.

ridft program of the TURBOMOLE package[36] with grid size m5 and the resolution-of-the-identity approximation of the Coulomb integrals (RI-J) in combination with the optimized auxiliary basis sets from References 37 and 38.

COSMO-RS as implemented in COSMO*therm* (version 2021)[39] has then been used to calculate the ground-state pK_a values in water at the BP-TZVPD-FINE level of theory following the protocol described in Hellweg and Eckert's work.[40] The optimized structures and energies of all conformers of the molecules in the test set at the BP-TZVPD-FINE level of theory are compiled as Table S1 of the Supporting Information (SI) and as xyz files in a Zenodo[41] repository.

1096987x, 2023, 24, Downloaded from https://onlinelibrary.wiley.com/doi/10.1002/jcc.27173 by Ruhr-Universität Bochum, Wiley Online Library on [09/10/2023]. See the Terms and Conditions (https://onlinelibrary.wiley.com/terms-and-conditions) on Wiley Online Library for rules of use; OA articles are governed by the applicable Creative Commons License

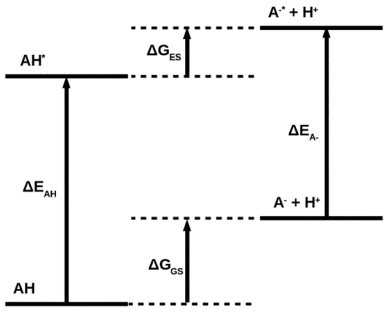


FIGURE 3 Förster cycle applied for the calculation of the excited-state acid strengths (pK_a^*). An upper index $*$ indicates electronically excited species. The lower indices GS and ES indicate, respectively, ground- and excited-state quantities.

For computing excitation energies, the ground-state geometries of all species have been re-optimized with the functionals used for the excitation energy calculations, that is, BP86, BLYP,[32,42] TPSS,[43] B3LYP,[44] PBE0,[45] M06-2X,[46] MN15,[47] CAM-B3LYP,[48] and ωB97X[49] in the def-TZVP basis for aqueous solution using TURBOMOLE's default parameters for the COSMO cavity construction and 78.3 for the dielectric constant of water.[35] At the wavefunction level we re-optimized the structures with COSMO-CC2[27] and COSMO-MP2[50] with the post-SCF reaction field scheme,[29] which for MP2 reduces to the perturbation on the energy (PTE) approach.[51] The COSMO-MP2 geometries have been used for the subsequent COSMO-ADC(2) calculations for excitation energies. Vertical excitation energies (VEE) have then been computed at the ground-state geometries with the same methods as used for the geometry optimizations using the def-TZVP and the larger def2-TZVPPD basis sets.[52] The COSMO-TD-DFT calculations used thereby the linear response reaction field scheme[53] and the COSMO-CC2 and COSMO-ADC(2) calculations the post-SCF scheme with a value of 1.3 for the refractive index of water.[54] All MP2, ADC(2), and CC2 calculations used the resolution-of-the-identity approximation[55-57] with optimized auxiliary basis sets[58,59] and the frozen core approximation with a $1s^2$ core at all C, N, and O atoms, a $1s^22s^22p^6$ core at Cl, and a $1s^22s^22p^63s^23p^63d^{10}$ core at Br.

Starting from the relation between the Gibbs free energy change ΔG upon proton transfer to the solvent and the acidity constant K_a:

$$\Delta G = -RT\ln K_a, \tag{1}$$

or the negative decadic logarithm of the latter

$$pK_a = -\log_{10}K_a = \frac{\Delta G}{RT\ln 10}, \tag{2}$$

the excited-state acidity strengths pK_a^* can, following the Förster cycle[8,9] (see Figure 3), be determined as:

$$pK_a^* = pK_a + \frac{(\Delta G_{ES} - \Delta G_{GS})}{RT\ln 10}. \tag{3}$$

In the last equation ΔG_{GS} and ΔG_{ES} are, respectively, the ground- and excited-state Gibbs free energy changes for proton transfer from the acid to water. Assuming that the entropy changes upon excitation are negligible, that is, $\Delta S_{ES} \approx \Delta S_{GS}$, we can approximate the difference between the Gibbs free energy changes by the differences in enthalpy $\Delta H_{GS} - \Delta H_{ES}$ which in turn are approximately equal to the differences between the excitation energies of the deprotonated and the protonated species ($\Delta E(A^-) - \Delta E(HA)$):

$$\Delta G_{ES} - \Delta G_{GS} \approx \Delta H_{ES} - \Delta H_{GS} \approx \Delta E(A^-) - \Delta E(AH). \tag{4}$$

The excited-state acid strengths are thus determined as:

$$pK_a^* = pK_a + \Delta pK_a^* = pK_a + \frac{\Delta E(A^-) - \Delta E(AH)}{RT\ln 10}. \tag{5}$$

The difference of excitation energies between conformers are negligible compared to the accuracy that can currently be achieved for excitation energies in solution. Therefore, we calculated the excitation energies only for the most stable conformer of each species. In equation 5, we used T equal to 298.15 K, R equal to 8.314 J mol^{-1} K^{-1},[60] and 1/(RT ln 10) equal to 16.9004 eV^{-1}.

3 | RESULTS AND DISCUSSION

3.1 | Calculation of ground-state pK_a

Tables 1 and 2 show a comparison between the pK_a values for the photoacids and photobases obtained with the COSMO-RS approach and experimental data from the literature. The absolute deviations of the computed from the experimental pK_a values are also shown in Figure 4. The computed values are mostly in good agreement with the experimental pK_a values: the mean absolute deviation (MAD) over the whole test set with both, photoacids and bases, is 0.53. Within the test set we observe for the acids a better agreement with the experimental values (MAD = 0.34 for pK_a) than for the bases (MAD = 0.74 for pK_a). The largest deviations between the calculated and the experimental pK_a values for acids and bases are found for, respectively, 5-*tert*-butyl-1-naphthol (0.75) and 5-aminoquinoline (1.47). These results show that COSMO-RS is a suitable method for predicting pK_a values for the compounds in our test set within about ± 1 pK_a unit.

3.2 | Excitation energy calculations

3.2.1 | Excited state assignments

The computed excitation energies in (eV), oscillator strengths, and NTOs of the lowest excited states in aqueous solution for the molecules in the test are made available under Zenodo.[41] For comparison with the experimental results one important step is to identify the lowest bright transition that is observed in the experimental spectrum.

1096987x, 2023, 24, Downloaded from https://onlinelibrary.wiley.com/doi/10.1002/jcc.27173 by Ruhr-Universität Bochum, Wiley Online Library on [09/10/2023]. See the Terms and Conditions (https://onlinelibrary.wiley.com/terms-and-conditions) on Wiley Online Library for rules of use; OA articles are governed by the applicable Creative Commons License

TABLE 1 pK_a values of the photoacids computed with the COSMO-RS approach compared with the corresponding experimental values.

Compounds	pK_a(*Exp.*)	pK_a(*Calc.*)	$\lvert pK_a(Calc.) - pK_a(Exp.)\rvert$
Phenol	9.99[a]	9.41	0.58
2-cyanophenol	6.97[b]	7.09	0.12
3-cyanophenol	8.34[b]	8.67	0.33
4-cyanophenol	7.74[b]	7.50	0.24
1-naphthol	9.4[c]	9.16	0.24
5-*tert*-butyl-1-naphthol	9.8[d]	9.05	0.75
5-cyano-1-naphthol	8.5[e]	8.39	0.11
2-naphthol	9.45[f]	9.41	0.04
5-cyano-2-naphthol	8.75[f]	8.94	0.19
3-hydroxycoumarin	6.95[g]	6.55	0.40
7-hydroxycoumarin	8[h]	7.36	0.6
7-hydroxy-4-methylcoumarin	7.78[i]	7.32	0.46
MAD/MAX error			
MAD (Acids)			0.34
MAX error (Acids)			0.75

[a]Taken from Reference 61.
[b]Taken from Reference 62.
[c]Taken from Reference 63.
[d]Taken from Reference 64.
[e]Taken from Reference 65.
[f]Taken from Reference 66.
[g]Taken from Reference 67.
[h]Taken from Reference 68.
[i]Taken from Reference 69.

TABLE 2 pK_a values of the photobases computed with the COSMO-RS approach compared with the corresponding experimental values.

Compounds	pK_a(*Exp.*)	pK_a(*Calc.*)	$\lvert pK_a(Calc.) - pK_a(Exp.)\rvert$
Quinoline	4.8[a]	5.63	0.8
5-cyanoquinoline	3.2[a]	3.33	0.1
5-chloroquinoline	3.8[a]	4.46	0.7
5-bromoquinoline	4.5[a]	4.32	0.2
5-methoxyquinoline	4.9[a]	5.93	1.0
5-aminoquinoline	5.3[a]	6.77	1.5
6-methoxyquinoline	5.2[b]	5.95	0.8
Acridine	5.62[c]	6.45	0.83
MAD/MAX error			
MAD (Bases)			0.7
MAX error (Bases)			1.5

[a]Taken from Reference 70.
[b]Taken from Reference 71.
[c]Taken from Reference 72.

The calculated excitation energies in (eV) for the def2-TZVPPD basis and the characters of the relevant transitions which have been used for calculating pK_a^* have been compiled in Table 3. The characters of the excited states were assigned based on available experimental data and the NTO analyses. Where experimental investigations did not specify a character for the excited state we assumed that the measured transition refer to the lowest excited state with a significant oscillator strengths at the CC2/def2-TZVPPD level of theory.

The experimental values for the absorption maxima in Table 3 for phenol and phenolate have been taken from Reference 73 and for the cyanophenols and the corresponding phenolate anions from Reference 62. For phenol and 4-cyanophenol it is known from experimental and computational results[73,74] that in aqueous solution the order of

1096987x, 2023, 24, Downloaded from https://onlinelibrary.wiley.com/doi/10.1002/jcc.27173 by Ruhr-Universität Bochum, Wiley Online Library on [09/10/2023]. See the Terms and Conditions (https://onlinelibrary.wiley.com/terms-and-conditions) on Wiley Online Library for rules of use; OA articles are governed by the applicable Creative Commons License

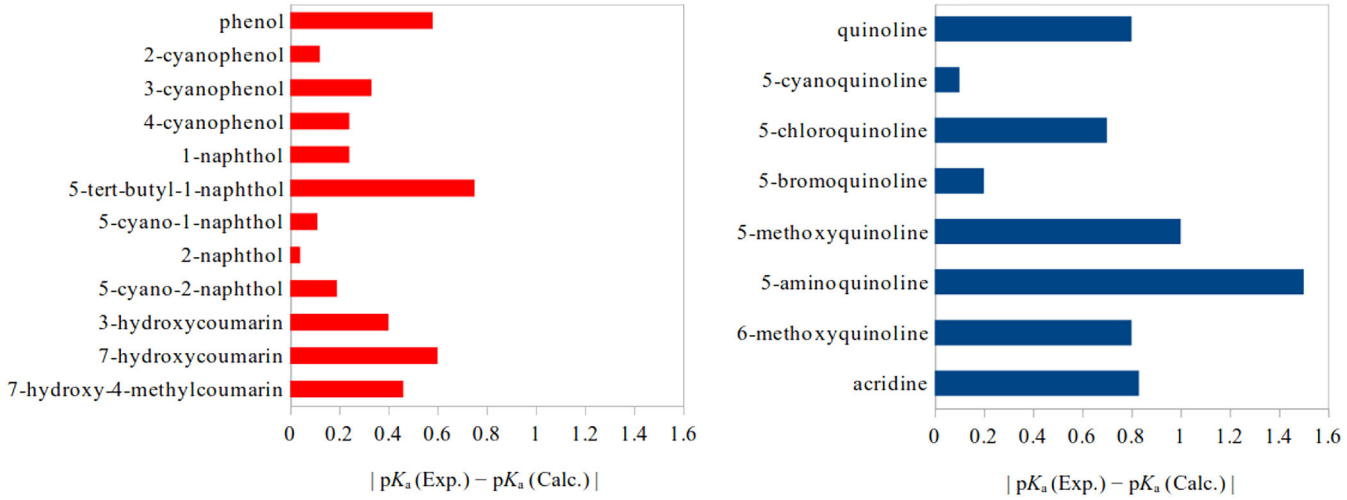


FIGURE 4 Absolute deviation of the pK_a obtained with COSMO-RS from the experimental values.

the two lowest $\pi \rightarrow \pi^*$ transition is $L_b < L_a$. For the respective anions Granucci et al. found in a theoretical investigation[74] that employed a mix of the double-ζ basis sets[75,76] cc-pVDZ and aug-cc-pVDZ an inversion of L_b/L_a. In the current work we found for phenolate and 4-cyanophenolate in the def-TZVP and def2-TZVPP basis sets in aqueous solution with all methods that L_b is below L_a in agreement with the assignment in the experimental study in Reference 62. For 2-cyanophenol and 3-cyanophenol the reduced symmetry of the π-system leads to a mix of L_b and L_a where the lowest excited state in the absorption spectrum has, however, still predominantly L_b character for both, the neutral and the anion species (cf. Table S3).

For 1-naphthol and 2-naphthol and the corresponding naphtholate anions, the experimental absorption maxima have been taken from References 77 and 78, for 5-*tert*-butyl-1-naphthol from Reference 7, the assignments as L_a or L_b have been done based on the NTO shapes[21]. For 1-naphthol and 5-*tert*-butyl-1-naphthol the first band in the absorption spectrum in aqueous solution is very broad[78,79] due to an overlap of L_a and L_b. The L_a transition has a much larger transition moment and is assigned to the maximum of the first band[7] and the L_b transition with a much smaller transition moment to a shoulder at the red end of the absorption spectrum.[7] From the computational methods used in the current study, only the ωB97X functional and the wavefunction-based methods ADC(2) and CC2 reproduce this order of the two lowest $\pi \rightarrow \pi^*$ transitions for 1-naphthol correctly (cf. Table 3). For 5-*tert*-butyl-1-naphthol only ADC(2) and CC2 reproduce the correct order. For 1-naphtholate and 5-*tert*-butyl-1-naphtholate, all methods reproduce correctly that the L_a band is the lowest $\pi \rightarrow \pi^*$ transition.[7]

On the other hand, for 2-naphthol and its conjugated base 2-naphtholate all computational methods applied, TDDFT as well as ADC(2) and CC2, give the L_b band as the lowest transition for the neutral form and reproduce the state inversion between the neutral and the deprotonated species.

For the cyanonaphthols, 5-cyano-1-naphthol and 5-cyano-2-naphthol, all computational methods predict L_a as the first state and that there is no state inversion when these molecules are deprotonated. Also for the hydroxycoumarins all the methods included in the current study reproduce the character of the first excitation as L_a and that of the second transition as L_b. For 7-hydroxycoumarin this observation is in line with the findings of a combined experimental and computational study of hydroxycoumarin derivatives.[80]

For all quinolines except 6-methoxyquinoline, the order of the two lowest $\pi \rightarrow \pi^*$ transition (L_a and L_b) of the neutral and cationic forms were assigned based on the experimental data[70] measured by steady-state and transient absorption and fluorescence spectroscopy techniques. For quinoline itself, the experimental data indicated that there is an overlap between the bands for L_a and L_b. We used the first excitation energy, which has L_a character, for the calculation of pK_a^*. For 5-cyanoquinoline, all computational methods except TDDFT with the BLYP and B3LYP functionals, predict in agreement with the literature[70] the order of the $\pi \rightarrow \pi^*$ transitions correctly (L_b more stable) and we found for this molecule a state inversion when it accepts a proton.

For acridine and acridinium in water, the experimental data indicates that the first excited state has L_a character with the absorption band maxima at 3.14 and 2.84 eV, respectively.[81,82] All computational methods give, in agreement with this, in water for both species as lowest excited state L_a, as revealed by the NTO analyses. This assignment is also in line with computational results by Rubio-Pons et al.[83] obtained with multistate complete active space second-order perturbation theory (MS-CASPT2) which support that in polar solvents $L_a < L_b$, as found in the current work. Since the L_a state is not only the lowest transition but also has the larger transition dipole moment, we used this state for the calculation of pK_a^*.

Table S2 in the Supporting Information summarizes the assignment of the excited states used for the pK_a^* calculations for all species included in the current work.

3.2.2 | Basis set and geometry effects on computed excitation energies

Apart from the electronic structure method, the one-electron basis set and the molecular geometry are important for the accuracy of the

1096987x, 2023, 24, Downloaded from https://onlinelibrary.wiley.com/doi/10.1002/jcc.27173 by Ruhr-Universität Bochum, Wiley Online Library on [09/10/2023]. See the Terms and Conditions (https://onlinelibrary.wiley.com/terms-and-conditions) on Wiley Online Library for rules of use; OA articles are governed by the applicable Creative Commons License

TABLE 3 Computed vertical excitation energies in (eV) obtained with the def2-TZVPPD basis set in water and characters of the transitions that have been used to determine the pK_a^* values.

Species	BLYP	B3LYP	CAM-B3LYP	PBE0	M06-2X	MN15	TPSS	ωB97X	CC2	ADC(2)	State	Exp
Phenol	4.70	5.04	5.21	5.15	5.29	5.15	4.86	5.25	4.94	4.95	L_b	4.59
Phenolate	3.91	4.25	4.44	4.35	4.53	4.38	4.05	4.49	4.11	4.10	L_a	4.32
2-cyanophenol	4.11	4.52	4.79	4.64	4.88	4.70	4.25	4.87	4.57	4.57	L_a	4.18
2-cyanophenolate	3.43	3.78	4.01	3.87	4.09	3.92	3.53	4.09	3.69	3.66	L_a	3.85
3-cyanophenol	4.05	4.49	4.78	4.61	4.89	4.70	4.18	4.86	4.57	4.57	L_a	4.22
3-cyanophenolate	3.11	3.55	3.88	3.67	4.01	3.80	3.22	3.99	3.60	3.57	L_a	3.90
4-cyanophenol	4.55	4.93	5.14	5.05	5.22	5.08	4.71	5.20	4.90	4.89	L_b	4.40
4-cyanophenolate	4.03	4.37	4.56	4.47	4.64	4.49	4.17	4.62	4.23	4.23	L_a	-
1-naphthol	3.98	4.31	4.55	4.42	4.58	4.45	4.12	4.60	4.29	4.31	L_b	3.86
1-naphthol	3.63	4.05	4.44	4.16	4.53	4.31	3.75	4.63	4.42	4.42	L_a	4.25
1-naphtholate	2.88	3.30	3.72	3.41	3.75	3.57	3.00	3.92	3.41	3.40	L_a	3.72[a]
5-*tert*-butyl-1-naphthol	3.94	4.27	4.50	4.37	4.53	4.39	4.07	4.57	4.21	4.23	L_b	
5-*tert*-butyl-1-naphthol	3.58	3.99	4.39	4.10	4.47	4.25	3.70	4.56	4.30	4.31	L_a	4.19
5-*tert*-butyl-1-naphtholate	2.91	3.33	3.74	3.44	3.76	3.58	3.03	3.93	3.38	3.37	L_a	3.72
5-cyano-1-naphthol	2.98	3.49	3.99	3.60	4.07	3.83	3.10	4.21	3.87	3.87	L_a	-
5-cyano-1-naphtholate	2.15	2.59	3.08	2.71	3.11	2.92	2.24	3.32	2.75	2.75	L_a	-
2-naphthol	3.69	4.08	4.39	4.18	4.45	4.28	3.81	4.51	4.18	4.19	L_b	3.79[a]
2-naphtholate	2.94	3.34	3.69	3.44	3.74	3.57	3.05	3.83	3.33	3.34	L_a	3.61[a]
5-cyano-2-naphthol	3.22	3.70	4.14	3.82	4.21	4.00	3.34	4.30	3.97	3.97	L_a	-
5-cyano-2-naphtholate	2.31	2.79	3.27	2.90	3.33	3.12	2.41	3.48	2.90	2.92	L_a	-
3-hydroxycoumarin	3.65	4.04	4.36	4.17	4.47	4.28	3.78	4.50	4.19	4.19	L_a	-
3-hydroxycoumarin (a)	3.12	3.52	3.83	3.65	3.95	3.76	3.25	3.98	3.54	3.48	L_a	-
7-hydroxycoumarin	3.58	3.99	4.32	4.12	4.39	4.21	3.71	4.47	4.09	4.11	L_a	-
7-hydroxycoumarin (a)	3.02	3.38	3.66	3.49	3.68	3.59	3.13	3.78	3.21	3.22	L_a	-
7-hydroxy-4-methylcoumarin	3.60	4.04	4.38	4.16	4.45	4.27	3.72	4.53	4.15	4.15	L_a	-
7-hydroxy-4-methylcoumarin (a)	2.98	3.37	3.70	3.49	3.72	3.58	3.09	3.85	3.21	3.25	L_a	-
Quinoline	3.90	4.31	4.73	4.45	4.83	4.59	4.03	4.91	4.69	4.71	L_a	-
Quinolinium	3.40	3.82	4.27	3.97	4.35	4.11	3.54	4.49	4.12	4.13	L_a	-
5-cyanoquinoline	4.03	4.37	4.64	4.48	4.62	4.59	3.91	4.66	4.35	4.35	L_b	-
5-cyanoquinolinium	3.37	3.84	4.30	3.99	4.39	4.19	3.50	4.50	4.22	4.20	L_a	-
5-chloroquinoline	3.66	4.12	4.56	4.24	4.65	4.42	3.79	4.78	4.51	4.52	L_a	-
5-chloroquinolinium	3.05	3.55	4.06	3.68	4.12	3.87	3.20	4.30	3.90	3.92	L_a	-
5-bromoquinoline	3.59	4.09	4.55	4.21	4.62	4.38	3.73	4.77	4.48	4.50	L_a	-
5-bromoquinolinium	2.93	3.47	4.02	3.61	4.07	3.81	3.09	4.28	3.86	3.88	L_a	-
5-methoxyquinoline	3.28	3.80	4.30	3.94	4.39	4.15	3.41	4.52	4.10	4.12	L_a	-
5-methoxyquinolinium	2.64	3.15	3.65	3.29	3.73	3.48	2.78	3.89	3.39	3.40	L_a	-
5-aminoquinoline	2.92	3.43	3.93	3.55	4.03	3.78	3.05	4.18	3.80	3.87	L_a	-
5-aminoquinolinium	2.24	2.69	3.17	2.81	3.25	2.99	2.36	3.43	3.01	3.09	L_a	-
6-methoxyquinoline	3.36	3.84	4.23	3.96	4.31	4.11	3.49	4.37	3.96	3.96	L_a	-
6-methoxyquinolinium	2.79	3.30	3.82	3.44	3.88	3.63	2.92	4.00	3.47	3.48	L_a	-
Acridine	2.86	3.23	3.65	3.33	3.70	3.48	2.95	3.86	3.56	3.55	L_a	3.14
Acridinium	2.65	3.01	3.42	3.11	3.44	3.25	2.75	3.62	3.20	3.17	L_a	2.84

Note: The experimental excitation energies refer to absorption maxima in aqueous solution. For coumarins the label "(a)" indicates the deprotonated anions.

1096987x, 2023, 24, Downloaded from https://onlinelibrary.wiley.com/doi/10.1002/jcc.27173 by Ruhr-Universität Bochum, Wiley Online Library on [09/10/2023]. See the Terms and Conditions (https://onlinelibrary.wiley.com/terms-and-conditions) on Wiley Online Library for rules of use; OA articles are governed by the applicable Creative Commons License

electronic excitation energies. To check the convergence of the excitation energies with respect to the basis set, we compared for all species the results in the def-TZVP and def2-TZVPPD basis sets (see Tables S4 and S5 in the SI). In addition, we examined for phenol and phenolate basis set effects beyond these two basis sets using the correlation-consistent basis sets[75,76,84] cc-pVTZ, aug-cc-pVTZ, cc-pVQZ, aug-cc-pVQZ, and aug-cc-pV5Z. Phenol and its conjugated base were selected since, on the one hand, phenol represents other photoacids relatively well and, on the other hand, very accurate experimental and theoretical gas phase data is available for this molecule: for example, in Reference 85 it has been shown that CC2 reproduces the experimental result for the 0–0 transition energy of phenol in the gase phase within a few hundredth of an eV. The results are compiled in Table S6 and Figure S1 of the SI. From the def-TZVP to the def2-TZVPPD basis the excitation energies for the lowest $\pi \rightarrow \pi^*$ transitions in the aromatic compounds decrease typically by 0.05 eV for TDDFT and 0.1 eV for the correlated wavefunction methods CC2 and ADC(2), but there are also a few cases where the changes are up to two times larger. On the other, a significant part of the changes with enlargement of the basis set cancel out for the differences between protonated and deprotonated species that enter ΔpK_a^*. For these differences the changes between the results in the def-TZVP and the def2-TZVPPD basis are in all cases below 0.1 eV (cf. Table S5) and the resulting basis set changes for ΔpK_a^* are at most 1.0 pK_a unit for the TDDFT calculations and slightly larger for CC2 (1.4 units) and ADC(2) (1.1 units). In most cases the results for ΔpK_a^* are in the larger basis more negative for the photoacids and more positive for the photobases, that is, the smaller basis underestimates the magnitude of the pK_a changes upon excitation by not fully capturing the differences between the protonated and deprotonated species. The larger basis set changes for the CC2 and ADC(2) results are not unexpected[86] as it is known that the second set of polarization functions included in def2-TZVPPD but not in def-TZVP is needed to achieve correlation-consistent triple-ζ quality.[87]

The remaining basis errors for the def2-TZPPD basis should be smaller than the changes between def-TZVP and def2-TZVPPD, as can be seen from the results for phenol and phenolate in the larger basis sets (Table S6). The results in the aug-cc-pVQZ basis are close to the basis set limit for all methods employed in the current study as can be seen by the negligible changes from aug-cc-pVTZ to aug-cc-pVQZ and aug-cc-pV5Z. From def2-TZVPPD to aug-cc-pVQZ the excitation energies decrease for phenol only by 0.01–0.03 eV and for phenolate by 0.02–0.05 eV. This leads to a further decrease of ΔpK_a^* from the def2-TZVPPD to the aug-cc-pVQZ basis by 0.2–0.5 units. Also the results for CC2 and ADC(2) don't change with these further basis set enlargements more than those for TDDFT which indicates that the def2-TZVPPD basis is sufficient for both, TDDFT and the wavefunction methods CC2 and ADC(2). From these findings we conclude that the deviations between the results in the def-TZVP and def2-TZVPPD basis are an upper limit for the remaining basis set errors in the def2-TZVPPD basis.

To test the sensitivity of the computed excitation energy differences between the protonated and deprotonated species to the geometry, we compared the results obtained for each method at the geometry optimized with same method in the def-TZVP basis with results obtained in single point calculations at the geometries obtained at the BP86/def-TZVP level of theory which has been used for the ground-state pK_a calculations. The results are compiled in Tables S7 and S8 in the SI. Among the density functionals, the changes to the geometries led to negligible changes (up to 0.03 eV) in the computed excitation energies for the GGA functional BLYP and the meta-GGA functional TPSS. This observation is rationalized by the fact that changes in equilibrium geometries between different GGAs and metaGGAs like BP86, BLYP, and TPPS are usually insignificant. However, for the hybrid functionals the changes are much more significant (up to $\approx$0.3 eV). For the wavefunction methods CC2 and ADC(2) the results are for most species less strongly affected by the geometry changes than for the hybrid functionals. There are, however, also exceptions like 5-aminoquinoline and 5-aminoquinolinium where the changes are also in the order of 0.2–0.3 eV. As for the changes with the basis set, also most of the changes with the geometry cancel out for energy differences between the protonated and deprotonated species. Thus, we do not see any unexpected geometry-sensitivity of the differences in the excitation energies between the acids and their conjugated bases that would suggest a need to use different methods for geometry optimization and excitation energy calculations.

3.2.3 | Comparison of computed excitation energies with absorption band maxima

For those species where experimental values for the absorption band maxima in water are available, we compare in Table 3 the computed vertical excitation energies with the band positions in water. This comparison contains already an inherent error since these quantities are not strictly comparable. In fact, in Reference 88 it is suggested to red shift vertical excitation energies by 0.1 eV to estimate the positions of band maxima. Table 4 lists the deviations between the computed VEEs and the experimental absorption band maxima.

In general, the absolute deviations found in this study for excitation energies in aqueous solution are a bit larger than expected for these methods in the gas phase,[85,89-92] even taking into account the inherent error of about 0.1 eV for the comparison of vertical excitation energies with band maxima. Most importantly, a striking difference between the results for the neutral photoacids and the anionic conjugated bases is observed. The correlated wavefunction methods CC2 and ADC(2) and TDDFT with most of the functionals overestimate the excitation energies of the neutral species (positive errors). Only the GGA functional BLYP underestimates them for two cases (2- and 3-cyanophenol) and the meta-GGA TPSS in one case (3-cyanophenol). Conversely, CC2 and ADC(2) underestimate in most cases the excitation energies for the anions (negative errors) as does also TDDFT with most of the functionals (BLYP, B3LYP, PBE0, MN15, and TPSS) in most cases. The functionals CAM-B3LYP, M06-2X, and ωB97X overestimate the excitation energies for almost all the species.

1096987x, 2023, 24, Downloaded from https://onlinelibrary.wiley.com/doi/10.1002/jcc.27173 by Ruhr-Universität Bochum, Wiley Online Library on [09/10/2023]. See the Terms and Conditions (https://onlinelibrary.wiley.com/terms-and-conditions) on Wiley Online Library for rules of use; OA articles are governed by the applicable Creative Commons License

TABLE 4 Deviations ($E_{vert} - E_{abs,max}$ in eV) between computed vertical excitation energies in the def2-TZVPPD basis and measured absorption band maxima in water together with the mean and the mean absolute deviations.

Species	BLYP	B3LYP	CAM-B3LYP	PBE0	M06-2X	MN15	TPSS	ωB97X	CC2	ADC(2)
Phenol	0.11	0.45	0.62	0.56	0.70	0.56	0.27	0.66	0.35	0.36
Phenolate	−0.41	−0.07	0.12	0.03	0.21	0.06	−0.27	0.17	−0.21	−0.22
2-cyanophenol	−0.07	0.34	0.61	0.46	0.70	0.52	0.07	0.69	0.39	0.39
2-cyanophenolate	−0.42	−0.07	0.16	0.02	0.24	0.07	−0.32	0.24	−0.16	−0.19
3-cyanophenol	−0.17	0.27	0.56	0.39	0.67	0.48	−0.04	0.64	0.35	0.35
3-cyanophenolate	−0.79	−0.35	−0.02	−0.23	0.11	−0.10	−0.68	0.09	−0.30	−0.33
4-cyanophenol	0.15	0.53	0.74	0.65	0.82	0.68	0.31	0.80	0.50	0.49
1-naphthol (L_b)	0.12	0.45	0.69	0.56	0.72	0.59	0.26	0.74	0.43	0.45
1-naphthol (L_a)	−0.62	−0.20	0.19	−0.09	0.28	0.06	−0.50	0.39	0.17	0.17
1-naphtholate	−0.84	−0.42	0.00	−0.31	0.03	−0.15	−0.72	0.20	−0.31	−0.32
5-*tert*-butyl-1-naphthol (L_a)	−0.61	−0.20	0.20	−0.09	0.28	0.06	−0.49	0.37	0.11	0.12
5-*tert*-butyl-1-naphtholate	−0.81	−0.39	0.02	−0.28	0.04	−0.14	−0.69	0.21	−0.34	−0.35
2-naphthol	−0.10	0.29	0.60	0.39	0.66	0.49	0.02	0.72	0.39	0.40
2-naphtholate	−0.67	−0.27	0.08	−0.17	0.13	−0.04	−0.56	0.22	−0.28	−0.27
MAD										
MAD (Neutral)	0.24	0.34	0.53	0.40	0.60	0.43	0.25	0.63	0.34	0.34
MAD (Anion)	0.66	0.26	0.07	0.17	0.13	0.09	0.54	0.19	0.27	0.28
MAD (Total)	0.42	0.31	0.33	0.30	0.40	0.29	0.37	0.44	0.31	0.32
Mean										
Mean (Neutral)	−0.15	0.24	0.53	0.35	0.60	0.43	−0.01	0.63	0.34	0.34
Mean (Anion)	−0.66	−0.26	0.06	−0.16	0.13	−0.05	−0.54	0.19	−0.27	−0.28
Mean (Total)	−0.37	0.03	0.33	0.14	0.40	0.22	−0.24	0.44	0.08	0.07

But also when the TDDFT results with a given functional deviate for the neutral form and its conjugated anion in the same direction from the experimental results it is always such that the excitation energies for the neutral forms have a larger blue shift (or smaller red-shift) than the results for the anions. This is a strong hint to a systematic imbalance in the description of the solvent effects by COSMO for (photo) acids and their anionic conjugated bases.

For gas phase calculations one would expect that among the density functionals the long-range corrected hybrid functionals ωB97X and CAM-B3LYP perform better than the global hybrids B3LYP, PBE0, M06-2X, and MN15 and the least performance for the meta-GGA TPSS and the GGA BLYP. GGAs and meta-GGAs underestimate often excitation energies, in particular if they have at least partially a charge-transfer character, while hybrid functionals typically overestimate excitation energies, depending on the amount of exact exchange. Indeed, we observe also for the excitation energies calculated in the current study in water in most cases that they increase in the order BLYP < TPSS < B3LYP ≤ ADC(2) ≈ CC2 < PBE0 < MN15 < CAM-B3LYP < M06-2X ≈ ωB97X and that the results for the global hybrids increase with the percentage of exact exchange (B3LYP 20% < PBE0 25% < MN15 44% < M06-2X 54%).

This trend leads for the neutral photoacids, for which in most cases all methods with the COSMO solvation model overestimate the lowest excitation energy, to MADs which are lowest for the GGA BLYP and mGGA TPSS, followed by CC2 and ADC(2) and are highest for the hybrid functionals with high percentage of exact exchange. Thus, among the hybrid GGA functionals, B3LYP gives for the neutral photoacids lower MADs than the PBE0 functional followed by MN15 and CAM-B3LYP and the largest deviations are found for M06-2X and ωB97X.

In contrast to the situation for neutral photoacids, the MADs follow a different order for the conjugated anionic bases, where the COSMO solvation model seems to result for water in excitation energies that are in almost all cases too much red-shifted. The MADs for the anionic bases are smallest for the hybrid functionals with high percentage of exact exchange (M06-2X, MN15, CAM-B3LYP, ωB97X) followed by PBE0 and B3LYP which use a smaller percentage of exact exchange and the highest MADs are obtained for the GGA BLYP and the meta-GGA TPSS. For the wavefunction-based methods the MADs for the neutral and anionic forms of the photoacids are close to each other (0.30 and 0.37 eV).

One possible explanation for these large differences in the deviations observed for the excitation energies of the neutral photoacids and their conjugated bases in water, which have not been observed to this extend in a recent study of hydroxypyrene-based photoacids in the aprotic solvent dimethyl sulfoxid[18] could be missing effects from hydrogen

1096987x, 2023, 24, Downloaded from https://onlinelibrary.wiley.com/doi/10.1002/jcc.27173 by Ruhr-Universität Bochum, Wiley Online Library on [09/10/2023]. See the Terms and Conditions (https://onlinelibrary.wiley.com/terms-and-conditions) on Wiley Online Library for rules of use; OA articles are governed by the applicable Creative Commons License

bonds not covered by the COSMO solvation model. Since by definition (photo)acids and their conjugated bases differ by the exchange of a hydrogen-bond donor with a hydrogen-bond acceptor site they are affected differently by specific contributions from hydrogen-bond interactions that are not captured by this continuum model.

3.2.4 | Phenol as test case for effects of hydrogen-bonding

To test the above hypothesis we used phenol as a prototypical test case. For phenol, but also for 1- and 2-naphthol, it has been shown before[85] that CC2 reproduces the S_1 0-0 transition energies in gas phase within >0.1 eV. We choose phenol and phenolate since they are the prototype for a large class of photoacids but still small enough so that results beyond DFT and the second-order wavefunction methods used here are available in the literature[74,93] for comparison. To obtain an estimate for the effects of including explicitly hydrogen bonds to the solvent, we optimized for phenol a microsolvated structure with a water molecule acting as hydrogen-bond acceptor and for the phenolate anion a structure with three water molecules acting as hydrogen-bond donors. The choice for the number and type of included hydrogen bonds is motivated by the Kamlet-Taft parameters for hydrogen-bond donation and acceptance strengths[94] according to which the OH group of phenol is a strong hydrogen-bond donor but only a week hydrogen bond acceptor. The O^- group in phenoxide can, on the other hand, accept up to three hydrogen bonds.[95] For the geometry optimizations and excitation energy calculations we followed the same protocol as as above, including COSMO to account for bulk solvation effects.

The results are summarized in Table 5. They show that the inclusion of explicit hydrogen-bonding blue shifts the excitation energy of the phenolate anion by about 0.3 eV while it red-shifts the excitation energy of phenol slightly by about 0.05 eV. This brings the results for both species closer to the experimental values, with remaining deviations from experiment that are now also for both cases positive, as expected for a comparison between vertical excitation energies and band maxima. This simple microsolvated cluster-continuum approach with a single structure per solvent can, of cause, not be expected to provide quantitative accuracy since it neglects structural fluctuations in the solvent shell. The latter would require averaging over a sufficiently large ensembles generated for example, with ab initio molecular dynamics which is beyond the scope of the current work. The above results, however, identify the explicit effects from hydrogen bonding as the dominant contribution to the remaining errors for the differences in the excitation energies for photoacids and their conjugated bases that enter in ΔpK_a^*.

3.3 | Acidity and basicity changes upon excitation: ΔpK_a^*

Also the experimental determination of pK_a^* or ΔpK_a^* is challenging because the short lifetime of the excited states prevents a direct measurement of ΔG_{ES} as thermodynamic equilibrium property. Instead, pK_a^* can be determined from kinetic measurements or ΔpK_a^* via the Förster cycle using either excitation energies taken from the absorption band maxima or the averages from the absorption and fluorescence band maxima as approximation for the 0-0 transition energies. In Table S9 of the SI we compiled experimental pK_a^* values from the literature for the photoacids and photobases studied in the current work. The values marked in Table S9 in bold font together with the experimental pK_a values listed in Tables 1 and 2 were used to convert between experimental pK_a^* and ΔpK_a^*.

The experimental values measured with the different approaches cover for some compounds a range of pK_a units especially for 1-naphthol and 2-naphthol, the classic examples of photoacids. These uncertainties make the comparison between experimental and computational pK_a^* values for some cases difficult. Apart from discrepancies between kinetic and spectroscopic measurements, also the different approximations for estimating the excited state energies like considering only absorption or emission or the average value which can lead to deviations between experimental values. Even the numerical uncertainty for the band maxima can affect ΔpK_a^* since a difference of 1 nm at 275 nm will change pK_a^* by $\approx$0.3 units.

On the other hand, the computational prediction of ΔpK_a^* is, as discussed above, limited by the accuracy with which solvent effects, in particular hydrogen bonds to the solvent, can be accounted for in the calculation of excitation energies. Crucial for the accuracy of ΔpK_a^* is the balanced description of the protonated and deprotonated species, which is challenging because the two differ in their charge, which has a decisive influence on the solvation energy, and their hydrogen-bond affinity. Even small errors in the computed excitation energy difference leads to a large error in pK_a^*: 0.1 eV error in the energy difference converts to an error of $\approx$1.7 units in pK_a^*.

For the above reasons one can for pK_a^* and ΔpK_a^* not expect the same degree of agreement between the experimental and computational results as for ground-state pK_a values. To benchmark the computational results we tried to select experimental pK_a^* values that are as comparable as possible with the computed results based on the following priorities:

1. Values determined via the Förster cycle using only the absorption band maxima. Where two or more experimental values were found, as for example, for 1-naphthol and 2-naphthol, the more recent results are used.
2. Values determined via the Förster cycle using the average of absorption and fluorescence band maxima. For the phenols where more than one experimental value has been published we took for consistency results from the same set of experiments reported in Reference 96.

Table 6 summarizes the computational results for ΔpK_a^*, the change in pK_a upon excitation, for the photoacids and photobases studied in this work in comparison with the experimental values. For the photoacids, we found above an overestimation of the excitation energies in water for the neutral acids and in general an

1096987x, 2023, 24, Downloaded from https://onlinelibrary.wiley.com/doi/10.1002/jcc.27173 by Ruhr-Universität Bochum, Wiley Online Library on [09/10/2023]. See the Terms and Conditions (https://onlinelibrary.wiley.com/terms-and-conditions) on Wiley Online Library for rules of use; OA articles are governed by the applicable Creative Commons License

TABLE 5 Vertical excitation energies (in eV) of phenol and phenolate with and without microsolvation (cluster-continuum) in comparison with the experimental band maxima in water.

	CC2		ADC(2)		
Species	**Continuum**	**Cluster-continuum**	**Continuum**	**Cluster-continuum**	**Exp.**
Phenol	4.94	4.87	4.95	4.89	4.59
Phenolate	4.11	4.44	4.10	4.42	4.32
$\Delta_{\text{phenol-phenolate}}$	0.83	0.43	0.85	0.45	0.27

TABLE 6 Computed ΔpK_a^* values for the photoacids and photobases in the def2-TZVPPD basis set in comparison with experimental results. The references and methods for the experimental values are given in Table S1 of the SI.

Compounds	ΔpK_a^* **(exp)**	**BLYP**	**B3LYP**	**CAM-B3LYP**	**PBE0**	**M06-2X**	**MN15**	**TPSS**	**ωB97X**	**CC2**	**ADC(2)**
Phenol	−7.0	−13.3	−13.4	−13.0	−13.5	−12.8	−13.1	−13.7	−12.8	−13.9	−14.4
2-cyanophenol	−7.5	−11.6	−12.6	−13.2	−13.1	−13.4	−13.2	−12.0	−13.1	−14.9	−15.4
3-cyanophenol	−7.3	−15.8	−15.9	−15.2	−15.8	−14.9	−15.2	−16.2	−14.7	−16.4	−16.8
4-cyanophenol	−4.5	−8.9	−9.5	−9.8	−9.7	−9.8	−9.9	−9.2	−9.8	−11.3	−11.1
1-naphthol	−8.7	−12.7	−12.7	−12.2	−12.7	−13.2	−12.6	−12.8	−12.1	−17.0	−17.1
5-*tert*-butyl-1-naphthol	−8.8	−11.3	−11.2	−10.9	−11.1	−11.9	−11.2	−11.2	−10.7	−15.5	−15.9
5-cyano-1-naphthol	−11.3	−14.2	−15.1	−15.3	−15.1	−16.1	−15.4	−14.4	−15.0	−18.9	−19.0
2-naphthol	−6.5	−12.6	−12.4	−11.8	−12.4	−12.0	−12.0	−12.8	−11.4	−14.3	−14.4
5-cyano-2-naphthol	−10.0	−15.4	−15.5	−14.7	−15.5	−15.0	−14.9	−15.7	−14.0	−18.0	−17.9
3-hydroxycoumarin	−4.4	−8.8	−8.8	−8.9	−8.7	−8.9	−8.7	−8.9	−8.8	−10.9	−11.9
7-hydroxycoumarin	−6.5	−9.4	−10.4	−11.2	−10.5	−12.0	−10.6	−9.7	−11.5	−14.8	−15.1
7-hydroxy-4-methylcoumarin	−6.9	−10.4	−11.2	−11.6	−11.3	−12.3	−11.6	−10.7	−11.5	−15.9	−15.1
Auinoline	6.7	8.5	8.3	7.7	8.1	8.1	8.1	8.3	7.1	9.7	9.7
5-cyanoquinoline	2.2	11.1	8.9	5.6	8.3	3.9	6.7	6.9	2.6	2.2	2.5
5-chloroquinoline	5.9	10.3	9.7	8.5	9.5	8.9	9.2	10.1	8.1	10.3	10.2
5-bromoquinoline	6.7	11.1	10.3	8.9	10.1	9.3	9.7	10.9	8.3	10.5	10.4
5-methoxyquinoline	10.2	10.8	11.1	11.0	11.0	11.2	11.3	10.8	10.6	12.1	12.2
5-aminoquinoline	10.6	11.6	12.5	12.9	12.5	13.1	13.2	11.7	12.7	13.4	13.1
6-methoxyquinoline	6.6	9.7	9.2	6.9	8.8	7.3	8.2	9.7	6.2	8.1	8.2
acridine	4.73	3.6	3.7	3.9	3.7	4.4	4.0	3.5	4.0	6.1	6.5

underestimation for the anionic bases which is caused by the replacement of a hydrogen-bond donating aromatic –OH group by an $-O^-$ group which accepts up to three hydrogen bonds. The effect of the latter is not fully captured by the COSMO solvation model and leads in total to a systematic overestimation of the excitation energy difference between the acids and their conjugated bases and, thus, a systematic underestimation of pK_a^*. For the photobases, the deviations between the computed and the experimental results for ΔpK_a^* are much smaller, in most cases the computed results overestimate the experimental values by a few pK_a units, much less than ΔpK_a^* is underestimated for the photoacids. This is consistent with the fact that for the studied photobases, quinolines and acridine, a site that can accept a single hydrogen-bond is replaced by a single hydrogen-bond donor site.

That the errors in the computed results for ΔpK_a^* is dominated by effects from hydrogen-bonding that are not captured by COSMO is corroborated by an analysis of possible error sources. Tables S10 and S11 in the SI list the changes of ΔpK_a^* between the def-TZVP and def2-TZVPPD basis sets for the whole test set and the changes with further basis set improvements for phenol is presented as Table S12. From the def-TZVP to the def2-TZVPPD basis ΔpK_a^* typically changes by 0.1 to 1.0 units. The test calculation for phenol indicate that the remaining basis set error in the def2-TZVPPD basis is for this photoacid about −0.5 pK_a units. This value will vary for the other studied species but are not expected to be much larger in magnitude. Anyway, in most cases the results for ΔpK_a^* decrease with basis set enlargement for the photacids and increase for the photobases. Thus, although remaining basis set errors are not fully negligible, they are not the most important contribution to the systematic deviations between the computed and experimental results for ΔpK_a^* since the latter even slightly increase with larger basis sets.

1096987x, 2023, 24, Downloaded from https://onlinelibrary.wiley.com/doi/10.1002/jcc.27173 by Ruhr-Universität Bochum, Wiley Online Library on [09/10/2023]. See the Terms and Conditions (https://onlinelibrary.wiley.com/terms-and-conditions) on Wiley Online Library for rules of use; OA articles are governed by the applicable Creative Commons License

Also, we do not find an extraordinary sensitivity of ΔpK_a^* on the molecular geometries: As one can see from Table S13, the changes between geometries optimized with DFT/BP86 and those optimized with the same method used for the excitation energies are in most cases below 1 pK_a unit.

To test the hypothesis that specific effects from hydrogen bonds between solute and solvent that are not captured by COSMO are the main source of error we had above calculated for CC2 and ADC(2) excitation energies with a microsolvated cluster-continuum model which includes explicit water molecules. In fact, we find that this brings the computed $\Delta\ pK_a^*$ value for phenol about seven pK_a^* units closer to experiment: from −13.9 and −14.4 for, respectively, pure COSMO-CC2 and COSMO-ADC(2) to −7.3 and −8.0 for, respectively, COSMO-CC2 and COSMO-ADC(2) with explicit water included. Compared to the experimental ΔpK_a^* value for phenol, −7.0, the CC2 and the ADC(2) results with COSMO and explicit water included overestimate the acidity increase upon excitation for phenol only by 0.3 and 1.0 pK_a units, respectively, which demonstrates the large effect of including the hydrogen bonding effects. That the inclusion of explicit water molecules improves the accuracy of pK_a calculations with implicit solvation models is known in the literature since some years for several examples including the COSMO-RS model used in the present work (see References 95,97,98 and references therein). The magnitude of the reported improvements for ground-state pK_a values are, however, smaller than the remaining errors found here for ΔpK_a^*. This might be related to the more diffuse orbitals that are occupied in electronically excited states which might make them more sensitive to specific solute-solvent interactions.

To account in the calculation of electronic excitation energies for the specific solvent effects from hydrogen bonds in protic solvents accurately and in a balanced manner for protonated and deprotonated species of acids and bases is challenging. This is in particular computationally demanding if accurate electronic structure methods need to be used to capture the differential effects from charge transfer and aromaticity change upon electronic excitation between acid and base forms. From the results in Table 6 it is apparent that the computed ΔpK_a^* values have for the photoacids a significant negative shift relative to the experimental ΔpK_a^* because the anions of the aromatic alcohols are strong hydrogen-bond acceptors while the neutral aromatic alcohols are hydrogen-bond donors. Furthermore, for the anions of the aromatic alcohols hydrogen bonds can influence the π system if oriented out-of-plane and, thus, significantly shift the $\pi\pi^*$ transitions from which the photoacidity in these systems originates. For the quinolines and the protonated cations hydrogen bonds should be oriented mostly in-plane with the aromatic system and have a smaller effect on the π electrons and the excitation energies. Within each of the two classes of compounds, however, one expects that the error caused by this for the excitation energy difference or for ΔpK_a^* is approximately proportional to ΔpK_a^* but mostly constant, that is, $\Delta pK_a^*\,(calc.) \approx c_0 + c_1 \cdot \Delta pK_a^*\,(exp.)$ with c_1 close to one. The results of such a correlation analysis which allows to separate such (and other) systematic errors from non-systematic errors related mostly to insufficiencies of the electronic structure methods are summarized in Table 7.

TABLE 7 Slopes, intercepts, and squared correlation coefficients for least square fits of linear relations, $\Delta pK_a^*\,(calc.) \approx c_0 + c_1 \Delta pK_a^*\,(exp.)$, between the experimental and computational values for the studied photoacids and photobases and various computational methods.

	Photoacids			Photobases		
Method	Slope	Intercept	R^2	Slope	Intercept	R^2
BLYP	0.84	−5.78	0.50	0.31	7.48	0.11
B3LYP	0.85	−6.04	0.56	0.6	5.20	0.40
CAM-B3LYP	0.77	−6.55	0.58	0.92	2.04	0.77
PBE0	0.84	−6.22	0.54	0.65	4.66	0.46
M06-2X	0.89	−6.03	0.75	1.07	1.11	0.87
MN15	0.83	−6.16	0.61	0.86	3.07	0.69
TPSS	0.83	−6.09	0.47	0.69	4.34	0.49
WB97X	0.70	−6.82	0.57	1.14	−0.19	0.90
CC2	1.12	−6.81	0.88	1.21	0.94	0.87
ADC2	1.07	−7.36	0.89	1.16	1.34	0.87

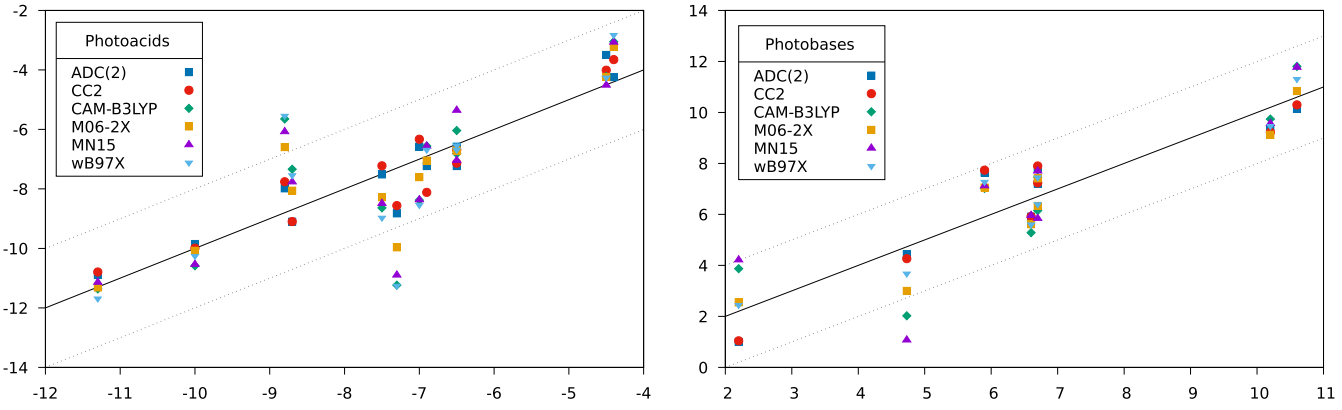


FIGURE 5 Comparison of ΔpK_a^* values calculated with the linear free energy relations in Table 7 with the experimental reference values. The dotted lines margin the range of ±2 pK_a units error.

1096987x, 2023, 24, Downloaded from https://onlinelibrary.wiley.com/doi/10.1002/jcc.27173 by Ruhr-Universität Bochum, Wiley Online Library on [09/10/2023]. See the Terms and Conditions (https://onlinelibrary.wiley.com/terms-and-conditions) on Wiley Online Library for rules of use; OA articles are governed by the applicable Creative Commons License

For the photobases we find in fact a good correlation with $R^2 \gtrapprox 0.8$ for CC2, ADC(2), and for DFT with the functionals with a high percentage of exact exchange M06-2X, ωB97X, and CAM-B3LYP with slopes (c_1) in the range of 0.92–1.21 and similar intercepts (c_0) between −0.19 (ωB97X) and 2.04 (CAM-B3LYP). Also the MN15 functional, which uses 44% of exact exchange, performs reasonably well for the photobases with $R = 0.69$. If applied analogously to the linear free energy relations that are used in the COSMO*therm* work protocols[40] for the prediction of ground-state pK_a to correct now the computed values for ΔpK_a^*, the corrected results for the photobases obtained for CC2, ADC(2), M06-2X, and ωB97X reproduce all experimental results within ±2 pK_a units (cf. Figure 5). For CAM-B3LYP and MN15 there is one outlier (acridine) with deviations larger than 2 pK_a units.

For the photoacids, the correlation is for some of the DFT functionals not as good, probably because the diversity of photoacids in the test sets (phenols, naphthols, hydroxycoumarins) is larger than for the photobases. We find a good correlation with $R^2 > 0.8$ for CC2, ADC(2), and still a decent correlation with $R^2 \gtrapprox 0.6$ for M06-2X, MN15, CAM-B3LYP, and B3LYP with slopes in the range of 0.70–1.12. As for the photobases, the wavefunction methods ADC(2) and CC2 reproduce for the photoacids all experimental values well with ±2 pK_a units (see Figure 5). The results for DFT significantly overestimate ΔpK_a^* for 5-*tert*-butyl-1-naphthol and significantly underestimate it for 3-cyanophenol. Strikingly, all three outliers that we find for the better performing DFT functionals, 5-*tert*-butyl-1-naphthol, 3-cyanophenol, and acridine belong to those cases where also the spread of the results for ΔpK_a^* in Figure 5within the DFT functionals is larger than on average in the test set. For 5-*tert*-butyl-1-naphthol—as for 1-naphthol—the large deviations between the DFT results can be traced back to an underestimation of the L_a transition energy in the neutral form that increases with decreasing exact exchange contribution in the exchange-correlation functional.[21] The same problem occurs for acridine.[99]

4 | CONCLUSIONS

In the current study we investigated systematically the capabilities and limitations for the prediction of excited-state acidities, pK_a^*, for a test set with typical photoacids and photobases with TDDFT and the second-order wavefunction methods CC2 and ADC(2) in combination with the COSMO solvation model as an example for a continuum solvation model. We have chosen this approach because of its computational efficiency which allows to apply it to a broad test set and also to larger molecules,[18] can be used with accurate electronic structure methods for excited states as for example, TDDFT with hybrid functionals and correlated wavefunction methods, and offers the perspective to include emission in solution.

An analysis of possible error sources for the absorption maxima in water for those compounds where experimental reference data is available revealed as the largest contribution to the errors solvent effects on the excitation energies that originate from hydrogen bonds between the photoacids and water that are not covered by COSMO. This error source is especially important for ΔpK_a^* because per definition acid and base form differ by the replacement of a hydrogen-bond donor by a hydrogen-bond acceptor site. To check to what extent the latter influences the results, we used phenol as a test case. We found that including one explicit water molecule as hydrogen-bond acceptor for the neutral form and three water molecules as hydrogen-bond donors for the phenolate anion in the COSMO calculations led to a significantly more accurate result for ΔpK_a^* of phenol. Thus, we can conclude that the prediction of pK_a^* values for photobases and photoacids in protic solvents with an accuracy that goes beyond that of the current study will require a systematic and balanced account of the effects of hydrogen bonding on the excitation energies.

A compromise is to correct for the remaining systematic errors via a linear relation with fitted empirical coefficients similar as it is used for the prediction of ground-state pK_a values with COSMO*therm*. This gives improved results that seem to be no longer limited in accuracy by the errors of the implicit solvation model, but by those of the underlying electronic structure methods and errors intrinsic to the comparison of vertical excitation energies with experimental results. One needs to keep in mind that usually the experimental pK_a^* values are determined by approximating 0-0 transition energies either by absorption or an average of absorption and emission energies.

With functionals that use a high percentage of exact exchange or correlated wavefunction methods the linear correction relation reproduces the experimental ΔpK_a^* values within about ±2 pK_a units or better, which is not far from the accuracy reached with COSMO*therm* for the ground-state pK_a values in water. DFT with pure GGA or mGGA functionals or hybrid functionals with a low percentage of exact exchange are, however, too inaccurate to reproduce more than very roughly the overall trends. Possibly, these functionals are not able to account accurately enough for differences in the changes in aromaticity upon electronic excitations in the chromophores between the protonated and deprotonated forms of photoacids and photobases.

AUTHOR CONTRIBUTIONS

Ali Ghiami-Shomami: COSMOconf and COSMOtherm calculations, COSMO geometry and excitation energy calculations, initial data analysis and visualization, initial manuscript draft. **Christof Hättig:** conceptualization, supervision, project administration, computational resources, cluster-continuum calculations, data analysis, curation and visualization, finalization of the manuscript.

ACKNOWLEDGMENTS

This project received funding from the European Union's Horizon 2020 research and innovation programme under the Marie Skłodowska-Curie grant agreement No. 801459 and the Deutsche Forschungsgemeinschaft (DFG) under Germany Excellence Strategy–EXC 2033–390677874–RESOLV. The authors declare that they have no competing financial interests. Open Access funding enabled and organized by Projekt DEAL.

1096987x, 2023, 24, Downloaded from https://onlinelibrary.wiley.com/doi/10.1002/jcc.27173 by Ruhr-Universität Bochum, Wiley Online Library on [09/10/2023]. See the Terms and Conditions (https://onlinelibrary.wiley.com/terms-and-conditions) on Wiley Online Library for rules of use; OA articles are governed by the applicable Creative Commons License

DATA AVAILABILITY STATEMENT

The primary data used for this study is available in the Supporting Information, a Zenodo[41] repository, or upon request from the authors.

ORCID

Christof Hättig https://orcid.org/0000-0002-5752-2710

REFERENCES

[1] O. Green, R. Simkovitch, L. Pinto da Silva, J. C. G. Esteves da Silva, D. Shabat, D. Huppert, *Chem. A Eur. J.* **2016**, *120*, 6184.
[2] Y. Liao, *Acc. Chem. Res.* **2017**, *50*, 1956.
[3] P. Cimino, U. Raucci, G. Donati, M. G. Chiariello, M. Schiazza, F. Coppola, N. Rega, *Theor. Chem. Accounts* **2016**, *135*, 16354.
[4] E. Pines, D. Huppert, N. Agmon, *J. Chem. Phys.* **1988**, *88*, 5620.
[5] N. Agmon, E. Pines, D. Huppert, *J. Chem. Phys.* **1988**, *88*, 5631.
[6] E. Pines, D. Huppert, *J. Am. Chem. Soc.* **1989**, *111*, 4096.
[7] E. Pines, *UV-Visible Spectra and Photoacidity of Phenols, Naphthols and Pyrenols*, Vol. 7, John Wiley & Sons, Ltd, Chichester **2003**, p. 491.
[8] T. Förster, *Naturwissenschaften* **1949**, *36*, 186.
[9] T. Förster, Z. Elektrochem, *Z. Angew. Phys. Chem.* **1950**, *54*, 42.
[10] Y. Houari, D. Jacquemin, A. D. Laurent, *Chem. Phys. Lett.* **2013a**, *583*, 218.
[11] Y. Houari, D. Jacquemin, A. D. Laurent, *Phys. Chem. Chem. Phys.* **2013b**, *15*, 11875.
[12] L. P. da Silva, J. C. G. Esteves da Silva, *ChemPhysChem* **2015**, *16*, 455.
[13] R. Hilal, S. G. Aziz, *Mol. Simul.* **2019**, *45*, 165.
[14] S. F. Alamudun, K. Tanovitz, A. Fajardo, K. Johnson, A. Pham, T. Jamshidi Araghi, A. S. Petit, *Chem. A Eur. J.* **2020**, *124*, 2537.
[15] S. F. Alamudun, K. Tanovitz, L. Espinosa, A. Fajardo, J. Galvan, A. S. Petit, *Chem. A Eur. J.* **2021**, *125*, 13.
[16] D. Jacquemin, E. A. Perpète, I. Ciofini, C. Adamo, *Chem. A Eur. J.* **2008**, *112*, 794.
[17] J. F. Joung, M. Jeong, S. Park, *Phys. Chem. Chem. Phys.* **2022**, *24*, 21714.
[18] N. Sülzner, C. Hättig, *Chem. A Eur. J.* **2022**, *126*, 5911.
[19] E. Runge, E. K. U. Gross, *Phys. Rev. Lett.* **1984**, *52*, 997.
[20] A. Dreuw, M. Head-Gordon, *Chem. Rev.* **2005**, *105*, 4009.
[21] A. Acharya, S. Chaudhuri, V. S. Batista, *J. Chem. Theory Comput.* **2018**, *14*, 867.
[22] P. G. Szalay, T. Watson, A. Perera, V. F. Lotrich, R. J. Bartlett, *Chem. A Eur. J.* **2012**, *116*, 6702.
[23] N. Agmon, *Chem. A Eur. J.* **2005**, *109*, 13.
[24] A. Klamt, G. Schüürmann, J. Chem, *Soc. Perkin Trans.* **1993**, *2*, 799.
[25] J. Schirmer, *Phys. Rev. A* **1981**, *26*, 2395.
[26] A. B. Trofimov, T. E. Moskovskaya, N. M. Vitkovskaya, J. Schirmer, *Zh. Fiz. Khim.* **1999**, *73*, 87.
[27] S. Karbalaei Khani, A. Marefat Khah, C. Hättig, *Phys. Chem. Chem. Phys.* **2018**, *20*, 16354.
[28] O. Christiansen, H. Koch, P. Jørgensen, *Chem. Phys. Lett.* **1995**, *243*, 409.
[29] S. Karbalaei Khani, A. Marefat Khah, C. Hättig, *J. Chem. Theory Comput.* **2020**, *16*, 4554.
[30] A. Klamt, *J. Phys. Chem.* **1995**, *99*, 2224.
[31] BIOVIA COSMOconf. Release 2021 dassault systémes, https://www.3ds.com
[32] A. D. Becke, *Phys. Rev. A* **1988**, *38*, 3098.
[33] J. P. Perdew, *Phys. Rev. B* **1986**, *33*, 8822.
[34] A. Schäfer, C. Huber, R. Ahlrichs, *J. Chem. Phys.* **1994**, *100*, 5829.
[35] C. G. Malmberg, A. A. Maryott, *J. Res. Natl. Bur. Stand.* **1956**, *56*, 1.
[36] TURBOMOLE, *V7.5 2020, a development of University of Karlsruhe and Forschungszentrum Karlsruhe GmbH 1989-2007, TURBOMOLE GmbH*, Karlsruhe **2007**, https://www.turbomole.org
[37] K. Eichkorn, O. Treutler, H. Öhm, M. Häser, R. Ahlrichs, *Chem. Phys. Lett.* **1995**, *240*, 283.
[38] F. Weigend, *Phys. Chem. Chem. Phys.* **2002**, *4*, 4285.
[39] BIOVIA COSMOtherm, *Release 2021; Dassault Systémes*, BIOVIA, Cologne **2021**, https://www.3ds.com
[40] A. Hellweg, F. Eckert, *AIChE J* **2017**, *63*, 3944.
[41] A. Ghiami-Shomami and C. Hättig (**2023**), https://doi.org/10.5281/zenodo.7792022
[42] C. Lee, W. Yang, R. G. Parr, *Phys. Rev. B* **1988**, *37*, 785.
[43] J. Tao, J. P. Perdew, V. N. Staroverov, G. E. Scuseria, *Phys. Rev. Lett.* **2003**, *91*, 146401.
[44] P. J. Stephens, F. J. Devlin, C. F. Chabalowski, M. J. Frisch, *J. Phys. Chem.* **1994**, *98*, 11623.
[45] C. Adamo, V. Barone, *J. Chem. Phys.* **1999**, *110*, 6158.
[46] Y. Zhao, N. E. Schultz, D. G. Truhlar, *J. Chem. Theory Comput.* **2006**, *2*, 364.
[47] H. S. Yu, X. He, S. L. Li, D. G. Truhlar, *Chem. Sci.* **2016**, *7*, 5032.
[48] T. Yanai, D. P. Tew, N. C. Handy, *Chem. Phys. Lett.* **2004**, *393*, 51.
[49] J.-D. Chai, M. Head-Gordon, *J. Chem. Phys.* **2008**, *128*, 084106.
[50] R. Cammi, B. Mennucci, J. Tomasi, *Chem. A Eur. J.* **1999**, *103*, 9100.
[51] F. del Valle, J. Tomasi, *Chem. Phys.* **1991**, *150*, 139.
[52] D. Rappoport, F. Furche, *J. Chem. Phys.* **2010**, *133*, 134105.
[53] M. Caricato, F. Ingrosso, B. Mennucci, J. Tomasi, *J. Chem. Phys.* **2005**, *122*, 154501.
[54] W. M. Haynes, D. R. Lide, T. J. Bruno, *CRC Handbook of Chemistry and Physics*, 97th ed., CRC Press, Florida **2016a**, p. 15.
[55] C. Hättig, F. Weigend, *J. Chem. Phys.* **2000**, *113*, 5154.
[56] C. Hättig, A. Hellweg, A. Köhn, *Phys. Chem. Chem. Phys.* **2006**, *8*, 1159.
[57] C. Hättig, *Adv. Quantum Chem.* **2005**, *50*, 37.
[58] F. Weigend, M. Häser, H. Patzelt, R. Ahlrichs, *Chem. Phys. Lett.* **1998**, *294*, 143.
[59] A. Hellweg, D. Rappoport, *Phys. Chem. Chem. Phys.* **2015**, *17*, 1010, https://doi.org/10.1039/C4CP04286G
[60] A. D. McNaught, A. Wilkinson, *Calixarene*, Blackwell Scientific Publications, Oxford **1997**.
[61] W. M. Haynes, D. R. Lide, T. J. Bruno, *CRC Handbook of Chemistry and Physics*, 97th ed., CRC Press, Florida **2016b**, p. 5.
[62] S. G. Schulman, W. R. Vincent, W. J. M. Underberg, *J. Phys. Chem.* **1981**, *85*, 4068.
[63] R. Bryson, A. Matthews, *Aust. J. Chem.* **1963**, *16*, 401.
[64] T. Barak, Ph.D. Thesis, *Ben-Gurion Univ. Negev* **2005**.
[65] E. Pines, D. Pines, T. Barak, B.-Z. Magnes, L. M. Tolbert, J. E. Haubrich, *Ber. Bunsenges. Phys. Chem.* **1998**, *102*, 511.
[66] L. M. Tolbert, J. E. Haubrich, *J. Am. Chem. Soc.* **1994**, *116*, 10593.
[67] P. M. Nowak, M. Woźniakiewicz, M. Piwowarska, P. Kościelniak, *J. Chromatogr. A* **2016**, *1446*, 149.
[68] D. W. Fink, W. R. Koehler, *Anal. Chem.* **1970**, *42*, 990.
[69] S. G. Schulman, L. S. Rosenberg, *J. Phys. Chem.* **1979**, *83*, 447.
[70] E. W. Driscoll, J. R. Hunt, J. M. Dawlaty, *J. Phys. Chem. Lett.* **2016**, *7*, 2093.
[71] O. Poizat, E. Bardez, G. Buntinx, V. Alain, *Chem. A Eur. J.* **2004**, *108*, 1873.
[72] A. Albert, J. N. Phillips, *J. Chem. Soc.* **1956**, 1294.
[73] E. F. G. Herington, W. Kynaston, *Trans. Faraday Soc.* **1957**, *53*, 138.
[74] G. Granucci, J. T. Hynes, P. Millié, T.-H. Tran-Thi, *J. Am. Chem. Soc.* **2000**, *122*, 12243.
[75] T. H. Dunning, *J. Chem. Phys.* **1989**, *90*, 1007.
[76] R. A. Kendall, T. H. Dunning, R. J. Harrison, *J. Chem. Phys.* **1992**, *96*, 6796.
[77] J. L. Rosenberg, I. Brinn, *J. Phys. Chem.* **1972**, *76*, 3558.

1096987x, 2023, 24, Downloaded from https://onlinelibrary.wiley.com/doi/10.1002/jcc.27173 by Ruhr-Universität Bochum, Wiley Online Library on [09/10/2023]. See the Terms and Conditions (https://onlinelibrary.wiley.com/terms-and-conditions) on Wiley Online Library for rules of use; OA articles are governed by the applicable Creative Commons License

[78] B.-Z. Magnes, N. V. Strashnikova, E. Pines, *Isr. J. Chem.* **1999**, *39*, 361.
[79] M. Prémont-Schwarz, T. Barak, D. Pines, E. T. J. Nibbering, E. Pines, *J. Phys. Chem. B* **2013**, *117*, 4594.
[80] V. F. Traven, L. I. Vorobjeva, T. A. Chibisova, E. A. Carberry, N. J. Beyer, *Can. J. Chem.* **1997**, *75*, 365.
[81] A. Weller, *Z. Elektrochem.* **1957**, *61*, 956.
[82] K. Kasama, K. Kikuchi, S. Yamamoto, K. Ujiie, Y. Nishida, H. Kokubun, *J. Phys. Chem.* **1981**, *85*, 1291, https://doi.org/10.1021/j150610a005
[83] O. Rubio-Pons, L. Serrano-Andrés, M. Merchán, *Chem. A Eur. J.* **2001**, *105*, 9664.
[84] F. Weigend, A. Köhn, C. Hättig, *J. Chem. Phys.* **2001**, *116*, 3175.
[85] A. Hellweg, S. A. Grün, C. Hättig, *Phys. Chem. Chem. Phys.* **2008**, *10*, 4119, https://doi.org/10.1039/B803727B
[86] A. D. Laurent, A. Blondel, D. Jacquemin, *Theor. Chem. Accounts* **2015**, *134*, 76.
[87] T. Helgaker, P. Jørgensen, J. Olsen, *Molecular Electronic-Structure Theory*, John Wiley & Sons, New York **2000**.
[88] S. Bai, R. Mansour, L. Stojanović, J. M. Toldo, M. Barbatti, *J. Mol. Model.* **2020**, *26*, 107.
[89] O. Christiansen, H. Koch, P. Jørgensen, J. Olsen, *Chem. Phys. Lett.* **1996**, *256*, 185.
[90] H. Koch, O. Christiansen, P. Jørgensen, J. Olsen, *Chem. Phys. Lett.* **1995**, *244*, 75.
[91] N. O. C. Winter, C. Hättig, *J. Chem. Phys.* **2011**, *134*, 184101, https://doi.org/10.1063/1.3584177
[92] R. Send, M. Kühn, F. Furche, *J. Chem. Theory Comput.* **2011**, *7*, 2376. https://doi.org/10.1021/ct200272b
[93] R. A. Livingstone, J. O. F. Thompson, M. Iljina, R. J. Donaldson, B. J. Sussman, M. J. Paterson, D. Townsend, *J. Chem. Phys.* **2012**, *137*, 184304.
[94] M. J. Kamlet, J. L. M. Abboud, M. H. Abraham, R. W. Taft, *J. Org. Chem.* **1983**, *48*, 2877.
[95] B. Thapa, H. B. Schlegel, *Chem. A Eur. J.* **2017**, *121*, 4698.
[96] S. Kaneko, S. Yotoriyama, H. Koda, S. Tobita, *Chem. A Eur. J.* **2009**, *113*, 3021.
[97] F. Eckert, M. Diedenhofen, A. Klamt, *Mol. Phys.* **2010**, *108*, 229.
[98] K. S. Alongi, G. C. Shields, *Annu. Rep. Computat. Chem.* **2010**, *6*, 113, https://www.sciencedirect.com/science/article/pii/S1574140010%060081
[99] A. Prlj, M. E. Sandoval-Salinas, D. Casanova, D. Jacquemin, C. Corminboeuf, *J. Chem. Theory Comput.* **2016**, *12*, 2652.

SUPPORTING INFORMATION

Additional supporting information can be found online in the Supporting Information section at the end of this article.

How to cite this article: A. Ghiami-Shomami, C. Hättig, *J. Comput. Chem.* **2023**, *44*(24), 1941. https://doi.org/10.1002/jcc.27173

1096987x, 2023, 24, Downloaded from https://onlinelibrary.wiley.com/doi/10.1002/jcc.27173 by Ruhr-Universität Bochum, Wiley Online Library on [09/10/2023]. See the Terms and Conditions (https://onlinelibrary.wiley.com/terms-and-conditions) on Wiley Online Library for rules of use; OA articles are governed by the applicable Creative Commons License